Asociación Argentina
de Mecánica Computacional

Mecánica Computacional Vol XXXIII, págs. 2565-2579 (artículo completo)
Graciela Bertolino, Mariano Cantero, Mario Storti y Federico Teruel (Eds.)
San Carlos de Bariloche, 23-26 Setiembre 2014

COMPARISON OF METALLURGICAL MODELS DURING QUENCHING USING OPEN SOURCE SOFTWARE

Humberto M. Celleri[a,b], Iván Viéitez Portela[c] and Diego N. Passarella[b]

[a]*Instituto J. Sabato, Comisión Nacional de Energía Atómica - Universidad Nacional de San Martín, Avenida General Paz 1499 - Partido de San Martín, Buenos Aires, Argentina, celleri@cnea.gov.ar, humberto.celleri@gmail.com, http://www.isabato.edu.ar*

[b]*Departamento de Ciencia y Tecnología, Universidad Nacional de Quilmes, Roque Sáenz Peña 352, B1876BXD Bernal Buenos Aires, Argentina, diego.passarella@unq.edu.ar, http://www.unq.edu.ar*

[c]*Departamento de Matemática Aplicada II, Escuela de Ingeniería de Telecomunicación, Universidade de Vigo, Campus de Vigo as Lagoas, Marcosende, s/n, 36310 Pontevedra, Vigo, España, ivanvieitez@yahoo.es, http://www.dma.uvigo.es*

Keywords: Quenching, Code_Aster, JMA-K, CCT diagram, TTT diagram.

Abstract. Quenching process is applied to steels pieces to improve their mechanical properties, enhance hardness and strength, obtaining desired microstructure distribution, while maintaining geometrical distortion and residual stresses within specification. This type of heat treatment is widely used in metal-mechanic industry.

The quenching process involves different physical fields: thermal, metallurgical and mechanical. Problem complexity increases as a consequence of physical fields interaction. Therefore, affecting mechanisms must be completely determined, and appropriate models elaborated if accurate predictions are pursued.

Waeckel's metallurgical transformation model is based on the numerical integration of the phase transformation's rate. Phase fraction evolution is solved by considering continuous cooling diagrams (CCT) and interpolating already known experimental thermo-metallurgical histories. On the other hand, Johnson-Mehl-Avrami-Kolmogorov (JMA-K) isothermal transformation model, is applied to continuous cooling by discretizing it as a succession of isothermal steps, in addition to an additivity rule to define the onset of transformation.

This article focuses on the resolution of an eutectoid steel piece. The effect of different metallurgical transformation models on final properties after quenching is assessed. Open-source thermo-mechanical and metallurgical software, Code_Aster, which already has Waeckel's transformation model built-in, is adapted to implement the JMA-K scheme.

1 INTRODUCTION

A simplified definition of a quenching process could be: a heat treatment process in which a component is rapidly cooled from a fully austenitic state, to obtain a narrow time window on which the desired metallurgical transformations are achieved, while maintaining geometrical distortion and residual stresses within specification. Although it may seem a simple process, quenching is one of the most complex processes in engineering, and one of the major causes of rejected components in the metallurgical industry. The final objective of a quenching process is to improve the component mechanical properties, such as strength, hardness and wear resistance.

Multiple physical fields has to be considered in the study of quenching: A thermal problem, which computes temperature evolution in a heat transfer process. A metallurgical problem, that involves micro-constituent transformations, and a mechanical problem, which concern stress and strains during quenching. The quenching simulation relies on accurate prediction of the temperature field, the most common approach to consider heat exchange during quenching is by using a heat transfer coefficient dependent on temperature. This allows to describe possible stages of cooling during the quenching process (vapor blanket, nucleate boiling, and convective cooling). Smoljan (2002) has previously used this approach to Jominy test simulation.

Metallurgical simulation during the quenching process has been studied in Waeckel (1994) and Denis et al. (1992). Generation of residual stresses and geometrical distortions are a complex phenomena reviewed in Leblond et al. (1986) and Leblond and Devaux (1989).

Fernandes and Denis (1986) proposed a mathematical model for coupling phase transformations with temperature evolution. Simsir and Gur (2010) used the JMA-K model to predict the thermo-metallurgical distribution and compute stresses on a hollow cylinder.

In this work, quenching process of a eutectoid steel cylinder is simulated. The thermal-metallurgical and mechanical fields are obtained with finite element solver *Code_Aster*. Software's source code is modified to implement a JMA-K anisothermal model. The same model is used to couple the heat released from metallurgical transformations in the thermal calculation. Thermo-metallurgical quenching path will determine the stress and strain results. Comparison between thermal, metallurgical and mechanical fields obtained with standard *Code_Aster*, anisothermal JMA-K, and coupled anisothermal JMA-K transformation models in the quenching process simulation of a eutectoid steel cylinder during quenching are presented.

2 MODELS

In this section, the mathematical models used for quenching process simulation are described. These models can be classified depending on the physical field they involve: thermal, metallurgical or mechanical model.

2.1 Thermal Model

The resolution of the thermal sub-problem assesses the temperature evolution within the steel piece volume (V) and in volume boundaries (∂V). Temperature evolution inside a solid is described by the heat conduction equation, which in its differential form for an axi-symmetrical geometry can be expressed as

$$\rho C_p \frac{\partial T}{\partial t} = \nabla \cdot (\lambda \nabla T) + Q \quad \forall \quad (r, z, t) \in \quad V \times (0, t_f) \tag{1}$$

where ρ, C_p and λ are material's density, specific heat and thermal conductivity. Q is a heat source. And the temperature evolution in volume's boundaries are computed with a flux rule

$$-\lambda\frac{\partial T}{\partial \bar{n}} = \Psi(T_s, T_\infty) \quad \forall \quad (r,z,t) \in \quad \partial V \times (0, t_f) \tag{2}$$

with Ψ a heat flux. In a quenching process, thermal properties are dependent on temperature and micro-structure fraction. A linear mixture rule is used. Every thermal property Υ of the mixture es calculated as

$$\Upsilon(T, \xi_k) = \sum_{k=1}^{N} \Upsilon_k(T)\xi_k \tag{3}$$

where Υ_k and ξ_k are the thermal property and the volume fraction of the k constituent.

The heat source Q is the volumetric enthalpy (ΔH_k) due to phase transformations,

$$Q = \sum_{k=1}^{N} \Delta H_k \dot{\xi_k} \tag{4}$$

with $\dot{\xi_k}$ the transformation rate of the k phase.

Other energy sources, such as the plastic-flow heat are neglected since they contribute less than one percent of the total during the quenching process [Sjöstrom (1985),Totten and Howes (2001)].

The initial and boundary conditions are assumed as

$$\begin{cases} T(r,t) = T_0 & \forall\,(r,t) \in (V,0) \\ -\lambda\frac{\partial T}{\partial \bar{n}} = 0 & \forall \quad \partial V_{sim} \\ -\lambda\frac{\partial T}{\partial \bar{n}} = h(T_s)(T_s - T_\infty) & \forall \quad \partial V_s \end{cases} \tag{5}$$

where T_0 is the initial temperature of the piece, set to austenization temperature. T_s is the nodal wall temperature and T_∞ is the quenching medium temperature. The surfaces in symmetrical boundaries, or those thermally isolated are represented with null outer flux. Heat transfer conditions for boundaries in contact with the quenchant are represented by a temperature dependent heat transfer coefficient $h(T)$. This coefficient allows to represent every fluid-solid heat transfer stage of the quenching process [Passarella (2012)].

2.2 Metallurgical Model

2.2.1 Diffusive Transformations

JMA-K: non isothermal model For anisothermal diffusional transformation to be simulated, the steel isothermal transformation diagram (IT diagram) and Scheil's additivity rule are applied. The nucleation of new phases is characterized by the incubation period, and the growing stage by the JMA-K coefficients. The incubation period is calculated using Scheil's additivity rule (equation 8), with $\tau(T_i)$ the isothermal incubation time.

$$S = \sum_{i=1}^{n} \frac{\Delta t}{\tau(T_i)} = 1 \tag{6}$$

where Δt is the time step used to temporally discretized the quenching process. In every time step, the process is assumed to proceed isothermally. In this work, the time step is constant:

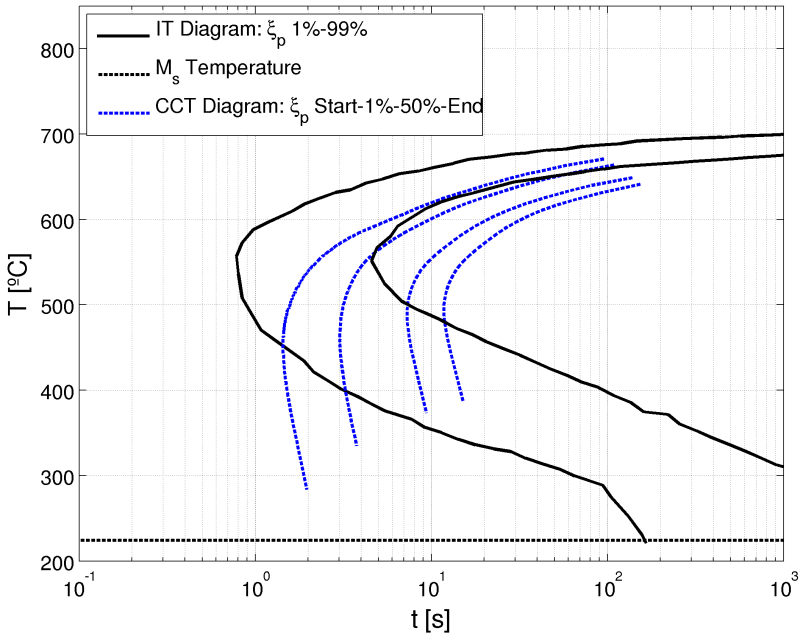

Figure 1: 1080 steel IT Diagram used for the quenching numerical simulation. Extracted from IT Diagrams Atlas. In blue, the CCT diagram obtained for constant cooling curves with JMA-K anisothermal model from the IT diagram.

1 hundredth of a second. Anisothermal growing stage is calculated with JMA-K isothermal model (equation 7) using the fictitious time concept (equation 8).

$$\xi_k^{t+\Delta t} = \xi_k^{max}(\xi_\gamma^t + \xi_k^t)(1 - exp(-b_k \cdot (t^* + \Delta t)^{a_k})) \tag{7}$$

with ξ_k^{max} the maximum fraction of the k micro-constituent, and ξ_γ^t, ξ_k^t the volume fractions of austenite and the k micro-constituent. For eutectoid steels, pearlite maximum fraction can be assumed as 1, since fully austenitic steels can transform completely to pearlite. The fictitious time is evaluated using the immediately previous time step micro-constituent volume fraction as

$$t^* = \left(-\frac{ln(1 - \xi_k(t))}{b_k} \right)^{\frac{1}{a_k}} \tag{8}$$

JMA-K coefficients $a(T)$ and $b(T)$ are temperature dependent parameters calculated from the eutectoid steel IT diagram (Figure 1). The expressions used are extracted from Kang and Im (2005). Resulting JMA-K $a(T)$ and $b(T)$ parameters are displayed in figure 2.

***Code_Aster*'s transformation model** $Code\_Aster$ uses Waeckel's transformation model, described in Waeckel (1994). During cooling processes, the metallurgical state is characterized by micro-constituent fractions (ξ_k), a number of principal variables (p) dependent on the previous thermal history, and a function (f) dependent on a finite number of principal and internal (η) variables.

$$\dot{\xi} = f(p, \dot{p}, \xi, \eta) \qquad\qquad \dot{\eta} = \Psi(p, \dot{p}, \xi, \eta) \tag{9}$$

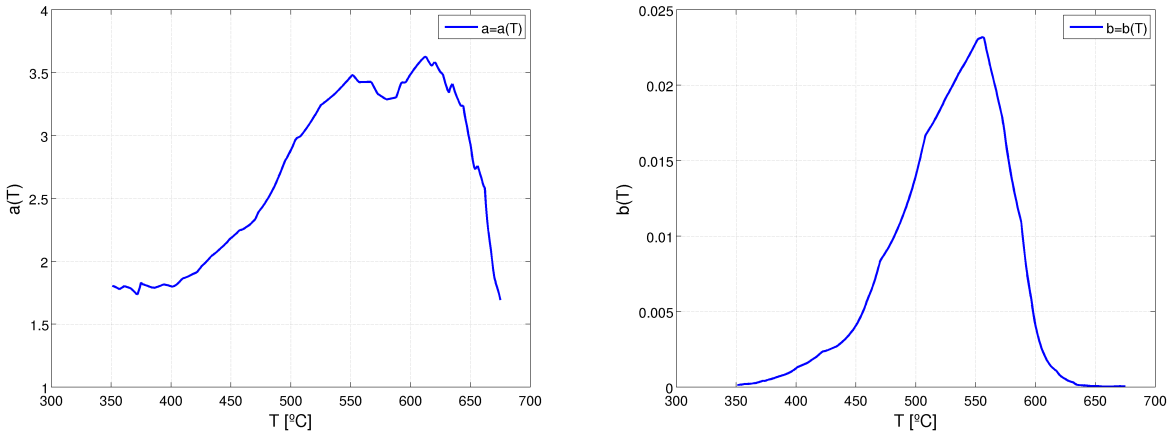

(a) (b)

Figure 2: JMA-K parameters a(T) and b(T), dependent on temperature.

Principal variables characterize the thermodynamic process, such as the temperature field (T) and its time derivative ($\dot{T}$). Austenitic grain size (d) can be included in the model as an internal variable. In this work the austenitic grain size is considered constant.

The difficulty to indicate a simple expression for the anisothermal phase transformation model led Waeckel to propose a differential equation with no particular analytical form, dependent on principal and internal variables,

$$\dot{\xi}(t) = f(T, \dot{T}, \xi, M_s; d) = f(T, \dot{T}, \hat{\xi}; d)\frac{\langle T - Ms \rangle}{T - Ms} \tag{10}$$

with $\hat{\xi}$ the constituents that transform with a diffusional mechanism, and $\langle X \rangle$ the positive part of X. The last term $\langle T - M_s \rangle$ states that under the martensitic transformation start temperature (M_s), there can not be any diffusional ones, this is considered as the independence rule for metallurgical transformations.

The data required is fully extracted from material's continuous cooling transformation (CCT) diagram. The CCT diagram is represented as a number of thermo-metallurgical histories, all of them assumed as particular solutions of the phase transformation differential equation 10. For each time step during the quenching process, the micro-constituent transformation velocities are obtained by numerical interpolation methods, which are then integrated to calculate the transformed fractions.

2.2.2 Non-Diffusional Transformations

The non-diffusional or displacive transformations such as the martensite transformation, are time independent transformations that occur under the martensite start temperature (M_s), assumed constant for the steel studied. Martensite fraction (ξ_m) is calculated with the Koïstinen-Marburger (KM) equation [Koistinen and Marburger. (1959)].

$$\xi_m = \xi_\gamma^0(1 - exp(-\beta[M_s - T])) \tag{11}$$

where ξ_γ^0 is the remaining austenite fraction, available for decomposition transformation. β is a material coefficient assumed constant.

2.3 Mechanical Model

The mechanical model computes the displacements (u_i), strains (ε_{ij}) and stresses (σ_{ij}) within the piece during the quenching process.

The most common causes of distortion and residual stresses are: internal stresses, thermal gradients and phase volume changes [Totten and Howes (2001)]. Internal stresses cause geometrical changes if exceed the yield strength. Thermal gradients causes stresses as a consequence of the different micro-constituent expansion coefficients. Each metallurgical phase has a particular crystallographic volume. During transformation, differences between specific volumes generate stresses.

In the quenching process, a high stress but small displacement relation occur. Under those assumptions the compatibility equations are those for small displacement used in De Vedia (1997). Assuming the strain tensor additive, the total strain is obtained as the sum of individual strains, each corresponding to a different physical deformation mechanism, and the strain rate is expressed as

$$\dot{\varepsilon}_{ij} = \dot{\varepsilon}^{e}_{ij} + \dot{\varepsilon}^{p}_{ij} + \dot{\varepsilon}^{th}_{ij} + \dot{\varepsilon}^{pt}_{ij} \tag{12}$$

where $\dot{\varepsilon}_{ij}$, $\dot{\varepsilon}^{e}_{ij}$, $\dot{\varepsilon}^{p}_{ij}$, $\dot{\varepsilon}^{th}_{ij}$ and $\dot{\varepsilon}^{pt}_{ij}$ are respectively the total, elastic, plastic, thermal and transformation plasticity contributions to the strain tensor. The classical elasto-plastic model without viscous effects, and considering Von Mises flow criterion with Prandt-Reuss flow rule is used to define the elastic and plastic problem, which can be seen in Vieitez Portela (2012) .

Materials mechanical properties change during the quenching process, they are functions of temperature and phase fractions. A common practice is to define a linear relationship for phase mixtures without austenite at low temperatures.

The hardening behavior is assumed as linear and isotropic for the Von Mises flow rule

$$\sigma_f = \sigma_0 + H\bar{\varepsilon}^{p} \tag{13}$$

where σ_f, σ_0 and H are the yield strength, the initial yield strength and the hardening coefficient respectively. $\bar{\varepsilon}^{p}$ is the accumulated plastic deformation.

The thermal strains for a phase mixture during the quenching process are obtained comparing against a metallurgical phase of reference at a temperature of reference (T_{ref}), in this case, the austenite. The strains are divided in those due to thermal expansion of austenite ($\varepsilon^{th}_{\gamma}$) and those generated by the resulting phases (ε^{th}_{f}).

The model, which includes the volumetric change between austenite and the resulting constituent ($\Delta\varepsilon^{T_{ref}}_{f_\gamma}$), can be described by

$$\varepsilon^{th}_{\gamma} = \alpha_\gamma(T)(T - T_{ref}) \tag{14}$$

$$\varepsilon^{th}_{f} = \alpha_f(T)(T - T_{ref}) + \Delta\varepsilon^{T_{ref}}_{f_\gamma} \tag{15}$$

where α is the thermal expansion coefficient. A linear mixture rule is used to obtain the total thermal properties as a function of different resulting constituents.

Transformation induced plasticity (TRIP) is known to produce plastic flow even far below the yield strength as a consequence of phase transformation submitted to stress states. The model for transformation induced plasticity was presented by Leblond and Devaux (1989).

$$\dot{\varepsilon}^{pt}_{ij} = \frac{3}{2}\sum_{k=1}^{N} K_k F'_k \dot{\xi}_k (1 - \xi_k) S_{ij} \tag{16}$$

where S_{ij} is the deviatoric part of the stress tensor, K_k are constants characteristic of the TRIP phenomenon, and F' is the derivative of a normalized function.

3 IMPLEMENTATION

The quenching process involves several coupled physical problems with different nature and mathematical behaviors. The problem is resolved using EDF's [1] open source finite element software *Code_Aster* [2] *v11.5*. Which is able to resolve a wide variety of thermo-mechanical problems.

Code_Aster resolution scheme is strictly sequential, it solves first the temperature field for all the computed times, then the metallurgical, and with the thermal and metallurgical fields, solves the stress and strain distribution. This scheme assumes implicitly that no heat is generated by phase transformations.A different resolution scheme is implemented to incorporate the metallurgical transformation heat source in the temperature evolution calculation.

The symmetry conditions of the geometry studied allows to use a 2D axisymmetrical simplification of the problem. The geometry and the mesh were made with *Salome*[3] software. A desktop computer with 8 core at 3.2 GHz and 8 GB of RAM memory was used to resolve the 60 seconds heat treatment problem, taking a time step of a hundredth of a second. The computation time was in the order of 2000 seconds.

The same spatial discretization is applied for every field computation. A quadrangular element mesh is employed with a number of approximately 1230 elements computed. Each quenching sub-problem is resolved for the same quadrangular mesh.

3.1 Thermal Problem

The temperature field is obtained resolving equation 1 by finite element method (FEM), using a implicit Euler integration method. Newton method with a maximum of 3 iterations is used for the non-linear thermal problem that arises from the temperature dependent materials properties and a MUMPS [4] (MUltifrontal Massively Parallel sparse direct Solver) solver, with convergence parameters set default, a global residual of $1.E-6$ and a maximum of 30 global iterations, to resolve the linear equations systems. The temperature of austenization, and the initial piece temperature, are set homogeneously to 830^oC. Boundary conditions can be divided on symmetry conditions and heat exchange conditions. Symmetry conditions are two, the first one is the axisymmetric axis ($\bar{Y}$ axis) and the medium length plane symmetry, $\bar{Z}\bar{X}$ plane at $Y = 30mm$. Those planes are thermally insulated. The heat exchange boundary condition is represented via a non-linear heat flux, calculated with a temperature dependent heat transfer coefficient $h(T)$. *Code_Aster* does not allow to include a temperature dependent heat transfer coefficient, the total heat fluxes must be introduced instead, calculated with equation 17.

$$q_s = h(T_s)(T_s - T_\infty) \tag{17}$$

q_s is the total heat flux, dependent on temperature. External boundaries have this condition.

[1] Electricité de France. http://france.edf.com/
[2] Electricité de France. http://www.code-aster.org/
[3] http://www.salome-platform.com
[4] http://mumps.enseeiht.fr/

3.2 Metallurgical Problem

The metallurgical field is described by each phase fraction. The simulation process start from a fully austenitic piece.

Code_Aster solves the metallurgical field differential equation by interpolating state variables such as the temperature, temperature time derivative, and phase fractions, with the 6 thermo-metallurgical histories that are linearly more close to the current state. This numerical method is highly precise for processes with cooling velocities similar to those applied to determine the CCT diagram [Waeckel (1996)]. The precision of the method is based on the number of thermo-metallurgical histories loaded in the CCT diagram. The smoothness of the solution also depends on the number of transformation values introduced for each thermo-metallurgical history. Computation time increases with the number of histories employed.

JMA-K model and the *KM* model are not partial differential equations, and so they can be solved using a progressive method, solving each time step with the previous step temperature field and phase fractions.

$$\xi_k(t + \Delta t) = \xi_k(t) + \Delta\xi_k \tag{18}$$

The metallurgical-thermal coupled model is resolved using a time displaced scheme (Equation 19). The heat source due to phase transformation is computed with one time step displacement, including the transformation heat released in next time step temperature computation. Since time step is small, the error is assumed to be small.

$$Q^{j+1} = f(\xi^j, \xi^{j-1}, T^j) \tag{19}$$

3.3 Mechanical Problem

Finally, its necessary to resolve the mechanical field with temperature and metallurgical results on every time step of the quenching process simulation. The stresses and strains are computed in *Code_Aster* using a elasto-plastic, isotropic linear hardening, with plastic transformation and hardening restoration. Mechanical models included in *Code_Aster*'s key word *META_P_IL_PT_RE*.

Hardening restoration is assumed to erase all the previous hardening when diffusional transformation take place, and to maintain all the hardening for displacive ones.

The non-linear plasticity problem is resolved using a iterative Newton method, the linear equation system for each load step is solved with a direct multi-frontal solver, with convergence parameters: global residual of $5.E-6$, and a maximum global iterations of 34. The boundary conditions are Dirichlet type, the displacement is restricted in the planes of symmetry, and particularly in the center of the geometry (corresponding to the origin of coordinates).

4 STUDY CASE

Different mathematical models has been used for the simulation of a quenching heat treatment. A simple geometry was studied, a cylinder. In section 5, thermal, metallurgical and mechanical evolution during the quenching process will be analyzed for two control points (core and surface showed in figure 3). The models used are: standard *Code_Aster* interpolative method, anisothermal JMA-K and a coupled JMA-K model. JMA-K model was introduced to *Code_Aster*'s source code as FORTRAN sub-routine.

The cylinder studied has 12.5 mm diameter and 60 mm high. A schematic sketch is shown in figure 3. The $\bar{Y}$ axis corresponds to the revolution symmetry axis. The origin of coordinates is in the core point.

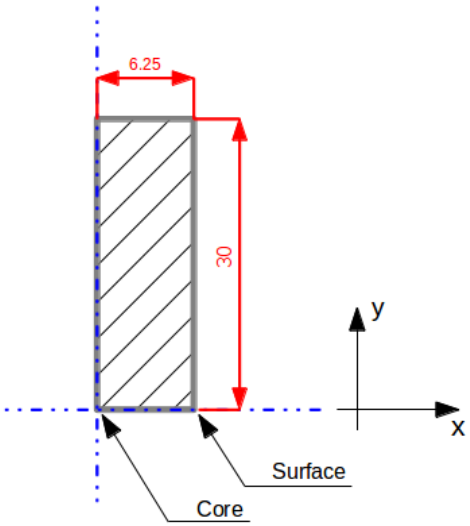

Figure 3: Schematic figure of the quenching cylinder.

The steel simulated is a numerically equivalent eutectoid steel with 0.79%C and 0.76%Mn, and a ASTM austenitic grain size 6. In eutectoid steels, austenite decomposes in pearlite, or martensite, depending on the cooling path of the quenching process. A_{r1} and M_s determines the temperature intervals in which the different transformations occur. These temperatures are obtain from the 1080 steel IT diagram [IT Diagrams Atlas]. A_{r1} temperature is 723^{o}C and M_S is considered equal to 224^{o}C .

Code_Aster does not allow to incorporate a temperature dependent heat transfer coefficient ($h(T)$). This is solved introducing a temperature dependent heat flux. The non linear heat flux condition used on the solid-quenchant exchange surfaces is represented in figure 4. Heat fluxes applied to simulate the quenching process were calculated with the heat transfer coefficient extracted from Smoljan (2002). This heat transfer coefficient can be associated with a Grossmann quenching severity $H = 0.2$.

4.1 Material Properties

In this section material properties used in the quenching simulation will be described. The lack of an open materials data source hinders obtaining the properties required. For this reason, properties not found for an eutectoid steel are replaced by similar steels grades properties. This work focuses on studying quenching model's behavior and the effect that metallurgical models generate on numerical results.

- Thermal properties needed are the specific heat (C_p), thermal conductivity (λ) and density (ρ) as a function of temperature. The values required were extracted from Kang and Im (2005) for a 0.80%C steel.

- Metallurgical properties are extracted from the isothermal transformation diagram (Figure 1). The IT diagram used was obtained from IT Diagrams Atlas for a 1080 grade steel. The CCT diagram needed to compute phase transformations with *Code_Aster* was calculated using JMA-K anisothermal transformation model. Thermo-metallurgical histories were recorded between 0.02 and 260 ^{o}C/s. The resulting CCT diagram is shown in figure 1.

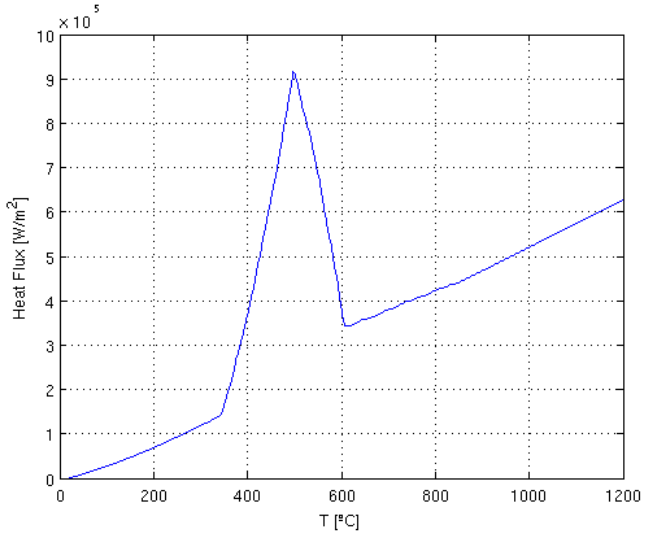

Figure 4: Heat flux applied to simulate the quenching process, calculated from a heat transfer coefficient extracted from Smoljan (2002).

- The mechanical problem needs several parameters. The number increases as the mechanical phenomenons to be taken into account. Mechanical properties can be distinguished between those for the mixture of phases (global properties), and those particular to the micro-constituent (local properties). In this work, a linear mixture rule is used to obtain global properties from local ones. In table 1 some local properties such as young modulus E, the Poisson coefficient ν, yield strength σ_y, hardening coefficient H and thermal expansion coefficient α are displayed as a function of temperature, the values were obtain from Simsir and Gur (2010). For TRIP parameters, the theoretical expressions presented by Leblond and Devaux (1989) are employed. TRIP function F and coefficient K are considered as

$$F(\xi) = \xi(1 - ln(\xi)) \tag{20}$$

$$K = \frac{2\Delta\varepsilon^{th}_{\gamma\to p/m}}{\sigma^{\gamma}_{y}} \tag{21}$$

where σ^{γ}_{y} is the yield strength of the austenite, and $\varepsilon^{th}_{\gamma\to p/m}$ is the difference of thermal deformation between the austenite, and the transformed phase.

5 RESULTS

In this section, the results of the quenching process simulation using different metallurgical transformation models in *Code_Aster* are stated. The conditions and parameters applied are described in sections 3 and 4. Temperature evolution, metallurgical fractions, stresses and strains are computed for a eutectoid steel cylinder quenching process. The results will be shown for two control points: the core of the piece, and a point located on the surface. The geometrical locations are displayed in figure 3.

The simulation was computed for the first 60 seconds of the quenching process. In figure 5 the thermal evolution for the coupled, and the uncoupled model are displayed. Temperature evolution for *Code_Aster*'s and JMA-K anisothermal model are identical (uncoupled). In the coupled scheme, the effect of the internal heat source due to phase transformations generate a

different temperature evolution, and as stated in Denis et al. (1987), it must not be neglected. Waeckel's interpolative method implemented in *Code_Aster* neglects this effect.

T(^{o}C)	E(GPa)	ν	σ_y(MPa)	H(MPa)	α(μm/^{o}C)
Austenite					
0	205	0.28	220	1000	23.5
300	185	0.30	130	16000	23.5
600	165	0.31	35	1000	23.5
900	124	0.35	35	500	23.5
Pearlite					
0	205	0.28	450	1000	15.0
300	185	0.30	230	16000	15.0
600	165	0.31	140	1000	15.0
900	124	0.35	30	500	15.0
Martensite					
0	205	0.28	1750	1000	15.0
300	185	0.3	1550	16000	15.0
600	165	0.31	140	1000	15.0

Table 1: Mechanical properties for a eutectoid steel [Simsir and Gur (2010)].

Figure 6 displays temperature and temperature time derivative evolution in the pearlitic transformation interval. Surface temperature is always below the core temperature. The temperature time derivative in figure 6a has two peaks that represent the maximum cooling rate on each point. Surface initially cools faster. After an inversion phenomenon of the cooling rate, the core cools faster than the surface. This phenomenon is well documented in Totten and Howes (2001). Temperature time derivative for the coupled model has a time window in which the cooling rate is negative. This is a recalescence phenomenon in which the piece actually increase its temperature due to phase transformation.

The pearlitic transformation during quenching is displayed in figures 7a, 7c and 7e for *Code_Aster*, JMA-K and JMA-K coupled model respectively. Figures will show the pearlitic transformation time interval. The complete metallurgical evolution can be found in Celleri (2014). Pearlitic transformation occurs between A_{r1} and M_s temperatures. Pearlite fractions between the standard *Code_Aster* and the JMA-K model differ by approximately 20%. The coupled model predicts a completely pearlitic core, and about 30% more pearlite in the surface. Transformations velocities are also displayed in figures 7a, 7c and 7e. Peaks represent the maximum pearlitic transformation rate.

Figures 7b, 7d and 7f display the tangential stress (σ_θ) evolution during the pearlitic transformation. The three transformation models generate a similar stress distribution. Initially, the rapid cooling on the surface generates a traction stress state, consequence of the thermal contraction. The core accordingly loads in compression. The stress evolves during the cooling process due to the temperature dependent expansion coefficient, until the pearlitic transformation occurs in the surface. Volume expansion due to phase transformation generates a rapid increase of the tension stress on the surface. After the core starts to transform, the stress state relaxes. The coupled scheme generates not only a fully pealitic core in the steel piece, but also a traction tension peak in the surface that exceeds 200MPa.

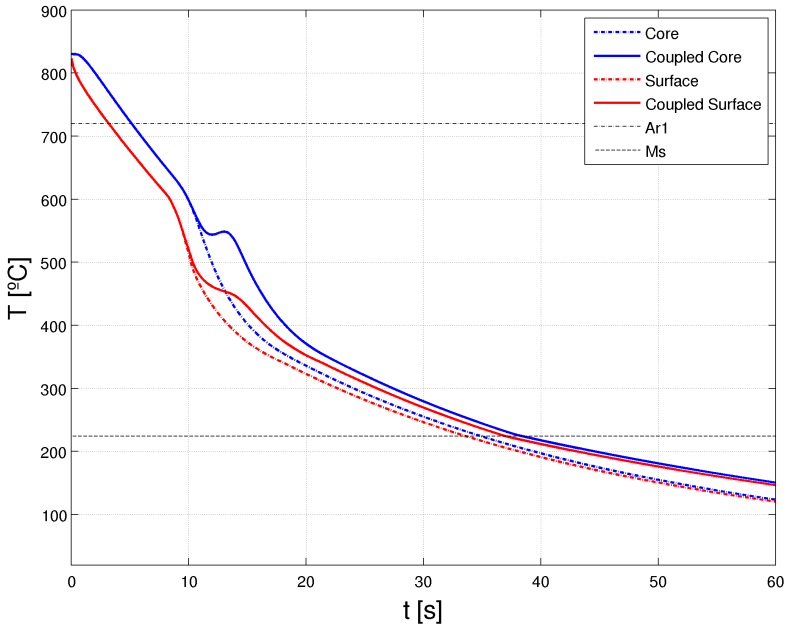

Figure 5: Temperature evolution during the quenching process for the coupled, and the uncoupled model.

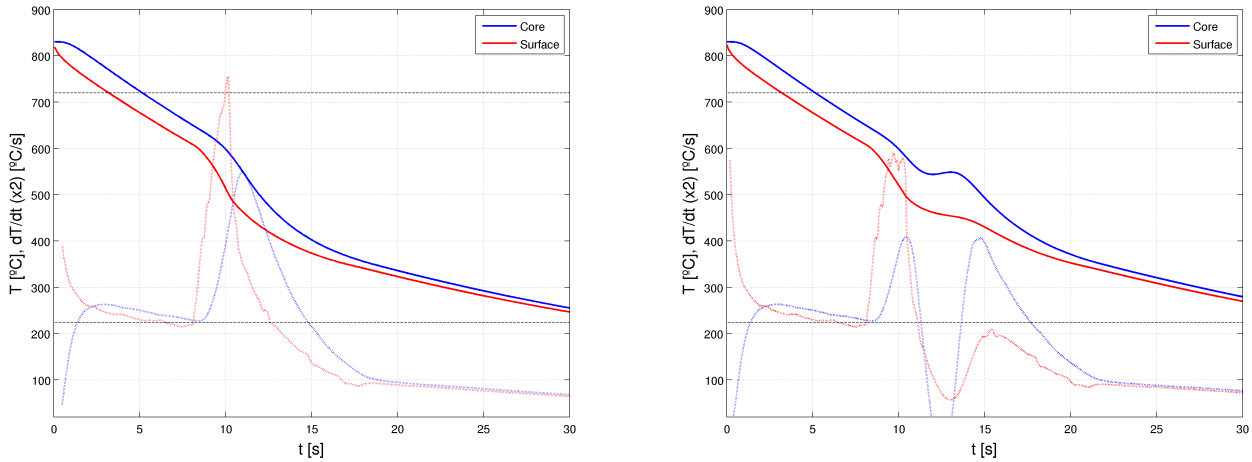

(a) *Code_Aster* and JMA-K (b) JMA-K coupled

Figure 6: Temperature and temperature time derivative evolution in the pearlitic transformation time interval.

The models studied could capture and reproduce the expected behaviors. Further work is needed, especially to compare with experimental data.

6 CONCLUSIONS

Quenching process of an eutectoid steel cylinder was studied by means of numerical simulation. The analysis was carried out with *EDF*'s open source software *Code_Aster*. As a result, temperature, phase fraction and stress evolution were determined.

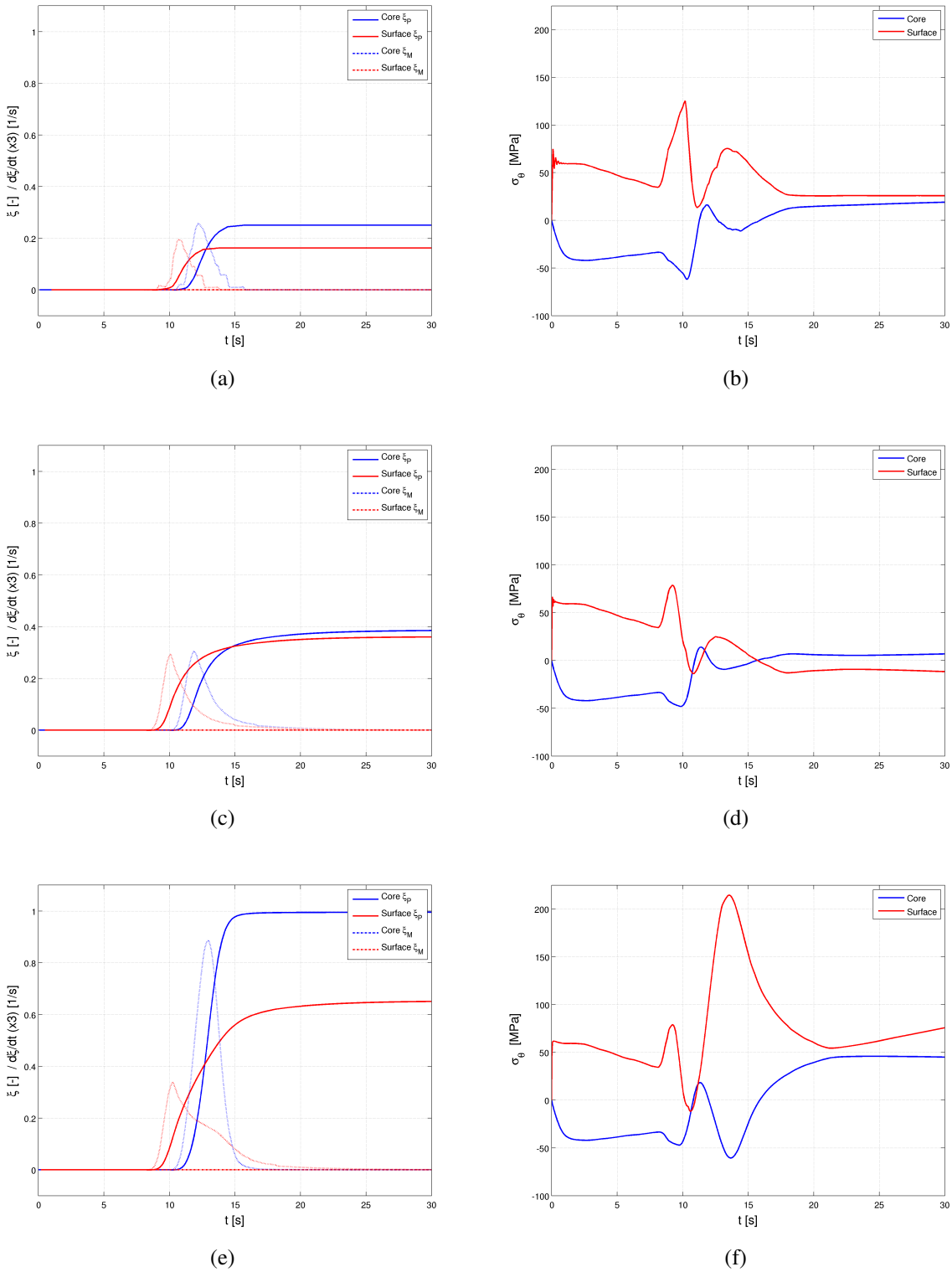

Figure 7: (a,b) *Code_Aster*'s model (c,d) JMA-K Model (e,f) JMA-K Coupled Model; Pearlite transformation distribution, and tangential stresses evolution.

The effect of three different metallurgical transformation conditions on final properties are assessed: first, the standard *Code_Aster* solver was employed to compute the quenching pro-

cess. *Code_Aster* has Waeckel's metallurgical transformation model built-in. The second transformation condition studied was Johnson-Mehl-Avrami-Kolmogorov (JMA-K) anisothermal model. For those two transformation conditions, thermal and metallurgical fields were first determined, and with the temperature and phase fractions evolution the mechanical field was computed. The third condition consists on the resolution of the coupled thermo-metallurgical field using the JMA-K anisothermal model, including the heat released during phase change in the thermal computation. The highly sequential *Code_Aster*'s thermo-metallurgical and mechanical resolution scheme was modified to implement a metallurgical and thermal coupled model.

As a consequence of the uncoupled formulation, the first two transformation conditions have identical thermal evolution, while the third condition presents a different thermal path resulting from the heat released due to phase transformation. The piece presents local recalescence. While phase fractions distribution are homogeneous, JMA-K model predicts approximately 20 percent more pearlite than *Code_Aster*'s model. The coupled model differs significantly, the cylinder is fully pearlitic in the core. The resulting stress state is highly dependent on the thermal and metallurgical evolution during the quenching process. The differences in the stress evolution for each metallurgical transformation condition are described. The coupled model generates traction stress peak due to pearlitic transformation in the surface.

JMA-K anisothermal transformation model and a coupled resolution scheme were implemented in *Code_Aster*. A steel cylinder quenching process was numerically simulated with them. Further work is needed, specially the acquisition of experimental data to compare and contrast the results obtained.

7 ACKNOWLEDGMENT

This work was partially funded by R&D grant Res. 673/13 of Secretaría de Investigación of Universidad Nacional de Quilmes. HMC acknowledges Universidad Nacional de San Martín for his graduate scholarship.

REFERENCES

Celleri H. *Modelado de Transformaciones Metalúrgicas durante Procesos de Temple utilizando Herramientas de Software Libre*. Deegre's thesis - Instituto de Tecnología Jorge Sabato: CNEA-UNSAM, 2014.

De Vedia L. *Mecánica del continuo*. Monografía tecnológica nro. 2: Instituto de Tecnología J. Sabato (CNEA-UNSAM), 1997.

Denis S., Farias D., and Simon A. Mathematical model coupling phase transformations and temperature. *Iron Steel Inst. Jpn. Int.*, 32:316–325, 1992.

Denis S., Sjöström S., and Simon A. Coupled temperature, stress, phase transformation calculation model numerical illustration of the internal stresses evolution during cooling of a eutectoid carbon steel cylinder. *Metallurgical Transactions A*, 18, 1987.

Fernandes F. and Denis S. Prévision de l'évolution thermique et structurale des aciers au cours de leur refroidissement condinu. *Memoires et etudes Scientifiques Revue de Métallurgie*, 1986.

IT Diagrams Atlas. *Atlas of Isothermal Transformation Diagrams*. United States Steel (USS), 1951.

Kang S. and Im Y. Three-dimensional finite-element analysis of the quenching process of plain-carbon steel with phase transformation. *Metallurgical and Materials Transactions A*,

36:2315–2325, 2005.

Koistinen D. and Marburger. R. A general equation prescribing the extent of the austenite-martensite transformation in pure iron-carbon alloys and plain carbon steels. *Acta Metallurgica*, 7:59–60, 1959.

Leblond J. and Devaux J. Mathematical modelling of transformation plasticity in steels i: Case of ideal-plastic phases. *International Journal of Plasticity*, 5:551–572, 1989.

Leblond J., Mottet G., and Devaux J. A theoretical and numerical approach to the plastic behavior of steels during phase transformations-ii. study of classical plasticity for ideal-plastic phases. *Journal of the Mechanics and Physics of Solids*, 34:411–432, 1986.

Passarella D.N. Cancelos R.V.I. Thermo-fluid-dynamics quenching model: Effect on material properties. *Blucher Mechanical Engineering Proceedings*, 1:3625–3644, 2012.

Simsir C. and Gur C. A simulation of the quenching process for predicting temperature, microstructure and residual stresses. *Journal of Mechanical Engineering*, 56:93–103, 2010.

Sjöstrom S. Interactions and constitutive models for calculating quench stresses in steel. *Materials Science and Tecnology*, 1:823–829, 1985.

Smoljan B. Numerical simulation of steel quenching. *Journal of Materials Engineering and Performance*, 11:75–79, 2002.

Totten G. and Howes M. *Handbook of Residual Stress and Deformation of Steel*. ASTM International, 2001.

Vieitez Portela I. *Modelización y cuantificación de las deformaciones producidas en el utilizaje de forja debido a los tratamientos térmicos*. Master's thesis - UDC-USC-UDV, 2012.

Waeckel E. Modélisation du comportement thermo-métallurgique des aciers. *Journal de Physique IV*, 4:221–226, 1994.

Waeckel E. A thermo-metallurgical model for steel cooling behaviour: Proposition, validation and comparison with the sysweld's model. *Journal de Physique IV*, 6:255–264, 1996.